Real-Time Optimal Switching Angle Scheme for a Cascaded H-Bridge Inverter using Bonobo Optimizer

Taha A. Taha [1*], Noor Izzri Abdul Wahab [2], Mohd Khair Hassan [3], Hussein I. Zaynal [4], Faris Hassan Taha [5], Abdulghafor Mohammed Hashim [6]
[1, 2, 3] Department of Electrical and Electronics Engineering, University Putra Malaysia (UPM), Serdang, Selangor 43400, Malaysia
[1] Unit of Renewable Energy, Northern Technical University, Kirkuk, Iraq
[4, 5] Computer Engineering Technology Department, Al-Kitab University, Altun Kupri, Kirkuk, Iraq
[6] Al-Amarah University College, Engineering of Technical Mechanical Power Department, Maysan, IRAQ
Email: [1] t360pi@gmail.com, [2] izzri@upm.edu.my, [3] khair@upm.edu.my, [4] drhussain.i.zainal@gmail.com, [5] f.h.aldabbagh@uomosul.edu.iq, [6] abd.ghafoor@alamarahuc.edu.iq
*Corresponding Author

***Abstract*—This study demonstrates a novel method for using the Bonobo Optimizer (BO) to selective harmonic elimination in a cascaded H-Bridge Multilevel Inverter (CHB-MLI) running on solar power. The primary objective is to calculate, in real time, the optimal switching angles for eliminating low-order harmonics while maintaining a constant output voltage despite variations in the input voltage. To prove that the BO algorithm works, tests were done on a three-phase, seven-level CHB-MLI that compared it to other evolutionary algorithms like the genetic algorithm (GA) and particle Swarm optimization (PSO). An adaptive BO-Artificial neural network (BO-ANN) based system was developed to compute real-time switching angles and applied to a 7-level CHB-MLI. The results demonstrate that the BO algorithm is the most accurate and fastest evolutionary algorithm for calculating optimal switching angles. This study illustrates the BO algorithm's effective utilization in real-time harmonic elimination applications in CHB-MLI.**

Keywords*—*Switching Angle Optimization; Bonobo Optimizer; Cascaded H-Bridge Inverter; Selective Harmonic Elimination; Renewable Energy.

I. Introduction

Multi-level inverters, especially Cascaded H-Bridge Multilevel Inverters (CHB-MLIs), have gained widespread adoption across various industries, offering enhanced efficiency, reduced switching losses, and superior electromagnetic compatibility compared to conventional two-level inverters. These inverters achieve their output waveform by combining different levels of direct current (DC) voltages to closely approximate a sinusoidal waveform [1]-[4].

Among the various inverter topologies available, CHB-MLIs stand out due to their modular structure and straightforward control mechanisms, making them preferable over alternatives like the Diode-clamped inverter and flying capacitor inverter [5]-[8].

CHB-MLIs are particularly well-suited for applications involving renewable energy sources such as solar photovoltaic (PV) systems. In this setup, each PV panel or series/parallel connected panels operates independently as a DC source for each bridge within the inverter system. The resulting staircase voltage output is a summation of voltages contributed by each individual bridge. Moreover, this arrangement eliminates the necessity for a transformer to amplify the voltage, as multiple bridges can be interconnected in series to achieve the desired output voltage level [9]-[13].

Reducing Total Harmonic Distortion (THD) is an essential design consideration for all multilayer inverters (MLI). Various control strategies and optimization methods have been proposed in the literature to reduce the THD of the output. The method of Selective Harmonic Elimination (SHE) is utilized to eradicate particular harmonics, as detailed in reference [14]-[20]. A proposed alternate strategy for eliminating lower-order harmonics involves the utilization of the Newton-Raphson (N-R) method, as outlined in references [2]. Nevertheless, the Newton-Raphson methods require a dependable initial approximation, as the solution would fail to converge otherwise. Furthermore, the computation of these non-linear transcendental equations necessitates a considerable computing endeavor, leading to a major expenditure of time. A strategy employing the idea of symmetrical polynomials has been outlined in [3] to mitigate the influence of higher-order harmonics and attain the desired output. Nevertheless, this approach is limited to a maximum of six switching angles. Furthermore, the current literature has applied both deterministic and stochastic techniques in [4], and curve fitting has been employed in [5] to tackle the SHE equations.

Many authors in the field of literature have employed evolutionary optimization approaches. The proposed optimization technique, presented in reference [21]-[28], employs evolutionary algorithms to minimize higher-order harmonics and maintain a constant value for the fundamental output voltage. However, the suggested method is constrained by the modulation index value throughout a wide spectrum. Reference [29]-[33] employs a combination of Genetic Algorithm (GA), Simulated Annealing (SA), and generalized pattern search as an alternative strategy. The red deer algorithm is proposed in [8]-[10] as a means of improving the switching angles. Furthermore, the literature discusses several evolutionary optimization methods, including Particle Swarm Optimization (PSO) [11] and a hybrid technique that combines PSO and Harmony Search [12].

Prior research [13] has utilized Artificial Neural Networks (ANN) to ascertain the ideal switching angles for reducing the THD of the output precisely. A graphical search strategy was utilized in [34]-[40] to mitigate the lower-order harmonics. In [41]-[44], a polynomial homotropy continuation method was used to solve the unified SHE equations. A unique power-sharing algorithm has been proposed in conjunction with the Selective Harmonic Elimination Pulse-Width Modulation (SHE-PWM) approach in reference to [45]-[48]. The research offers a comprehensive analysis of several evolutionary techniques utilized for minimizing harmonics, as stated in references [49]-[65].

This study employs the Bonobo Optimizer (BO), a newly developed optimization technique, to optimize the switching angle for a CHB-MLI with unequal input DC voltages. This optimization renders the CHB-MLI suitable for photovoltaic (PV) based applications. Compared to alternative algorithms such as GA and PSO, the BO method has superior speed and resilience. Once the optimal firing angles are determined for different input voltages, this data is used to train the artificial neural network (ANN), which will then create the switching angles in real time. The simulation results are compared to other methods, and an experimental setup has been created to confirm the effectiveness of the proposed strategy.

The next sections of the paper are organized in the following manner. Sections 2 offer a detailed description of how the cascaded H-bridge inverter operates and how it can be used with unequal Direct Current (DC) voltage sources. The BO has been explained in Section 3, while the proposed technique has been described in detail in Section 4. Section 5 presents the simulation findings and conducts a comparative analysis with alternative evolutionary approaches. Section 6 of the study presents the introduction of the ANN-based adaptive switching angle technique, followed by the presentation of concluding remarks in Section 7.

II. CASCADED H-BRIDGE INVERTERS

Fig. 1 displays the configure ration of a 7-level CHB inverter with three phases. The system comprises three H-bridge cells connected in series in each phase. Each bridge can produce three voltage levels: $+Vdc$, 0, $-Vdc$. The output staircase voltage will be 2m + 1 level, where m represents the combined number of H-bridge cells and DC sources. When three H-bridges are connected in series, the resulting output voltage waveform will exhibit seven distinct levels, as depicted in the accompanying diagram. The primary benefits of this topology include a modular structure, straightforward protection, and convenient modulation control. However, unlike other topologies, such as the diode-clamped bridge, the CHB inverter necessitates independent DC sources for each bridge. In CHB-MLI, low-frequency square wave modulation achieves more minor switching losses. In addition, this modulation method makes the implementation fast and straightforward.

A. Selective Harmonic Elimination

A very popular way to get rid of the lower order harmonics from the output of the CHB-MLI is to use SHE-PWM. With SHE, switching losses are very low because devices only need to be moved twice during a switching cycle. This makes SHE better than other PWM methods. SHE equations with three independent angles for the seven-level inverter case are given in equation (1). One of the angles controls the fundamental voltage, while the remaining angles are used to eliminate selected harmonics.

$$\begin{aligned} cos(\theta_1) + cos(\theta_2) + cos(\theta_3) &= 3m \\ cos(5\theta_1) + cos(5\theta_2) + cos(5\theta_3) &= 0 \\ cos(7\theta_1) + cos(7\theta_2) + cos(7\theta_3) &= 0 \end{aligned} \quad (1)$$

B. CHB Inverter with Unequal DC Sources

The input isolated dc sources may not be constant and equal every time in many real-world applications. A CHB that is powered by PV panels instead of continuous dc sources is one example of this kind of application. Fig. 2 shows the typical P-V characteristic of the PV module for different temperature and irradiance values. It can be seen that the position of the MPP changes as a function of radiation and temperature. Fig. 2(a) shows the P-V curve of the PV panel under the irradiation value varying from 0.1 p.u. to 1 p.u. It can be seen from the Fig. 2 that the Vmpp value also varies between 33V and 35V for the given range of irradiation values. Fig. 2(b) shows the P-V curve of the panel at 50C to 500C, with varying panel temperatures. It can be seen from the Fig. 3 that the Vmpp value also varies between 32V and 38V for the given temperature range. If ΔV is the voltage change due to a single panel, and Ns is the number of panels connected in series, the change in voltage is given as in Equation (2).

$$\Delta V_T = N_s \times \Delta V \quad (2)$$

The output voltage rms value and the shape of the output voltage waveform are constantly changing due to these variable input voltages, leading to the very undesirable scenario of poor power quality from the system. The staircase waveform of the output for the uneven dc-voltages may be represented using Fourier analysis as in Equation (3).

$$\begin{aligned} &V_{\text{ab}}(\omega t) \\ &= \sum_{n=1,3,5\ldots}^{\infty} \frac{4}{n.\pi} \times [V_{\text{PV1}}\, cos(n\theta_1) + \text{V}_{\text{PV2}}\, cos(n\theta_2) \\ &+ V_{\text{PV3}}\, cos(n\theta_3)] \times [sin(nwt)] \end{aligned} \quad (3)$$

Where, V_{PV_1}, V_{PV_2}, and V_{PV_3} are DC input voltages (PV panel voltages). θ_1, θ_2, and θ_3 are switching angles, and due to quarter-wave symmetry, the switching angles must satisfy the condition in Eq. (4).

$$0 \le \theta_1 < \theta_2 < \theta_3 \le \frac{\pi}{2} \quad (4)$$

In a balanced three-phase system, harmonics of three and a multiple of three can be neglected at interphase voltages. In this case, minimizing the 5th, and 7th order lower harmonics is sufficient. If the set of equations is rearranged as follows:

$$V_{\text{fund}} = V_{\text{PV1}} \cos(\theta_1) + V_{\text{PV2}} \cos(\theta_2) + V_{\text{PV3}} \cos(\theta_3)$$
$$V_{5th} = V_{\text{PV1}} \cos(5\theta_1) + V_{\text{PV2}} \cos(5\theta_2) + V_{\text{PV3}} \cos(5\theta_3) \quad (5)$$
$$V_{7th} = V_{\text{PV1}} \cos(7\theta_1) + V_{\text{PV2}} \cos(7\theta_2) + V_{\text{PV3}} \cos(7\theta_3)$$

In this work, we provide an approach for determining the best switching angles that minimize THD while keeping the output voltage where it needs to be. In order to do this, we have created an optimization problem and established the corresponding constraints. THD and selective total harmonic distortion (THDe) values in three-phase systems may be determined using Eq. (6) and (7), respectively.

$$THD = \frac{\sqrt{V_5^2 + V_7^2 + V_{11}^2 + \cdots}}{|V_1|} \quad (6)$$

$$THDe = \frac{\sqrt{V_5^2 + V_7^2}}{|V_1|} \quad (7)$$

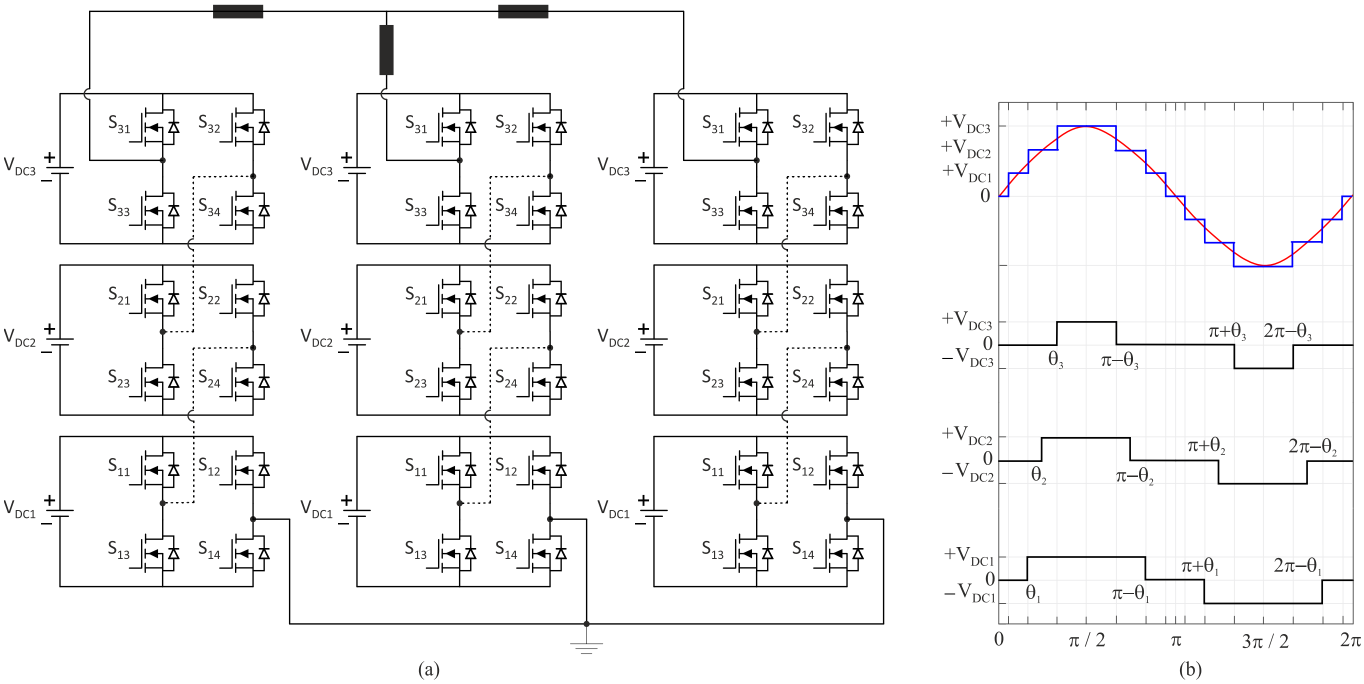

Fig. 1. Configure ration of 7-level 3-phase CHB-MLI: a) Circuit and b) Single-phase output voltage waveform

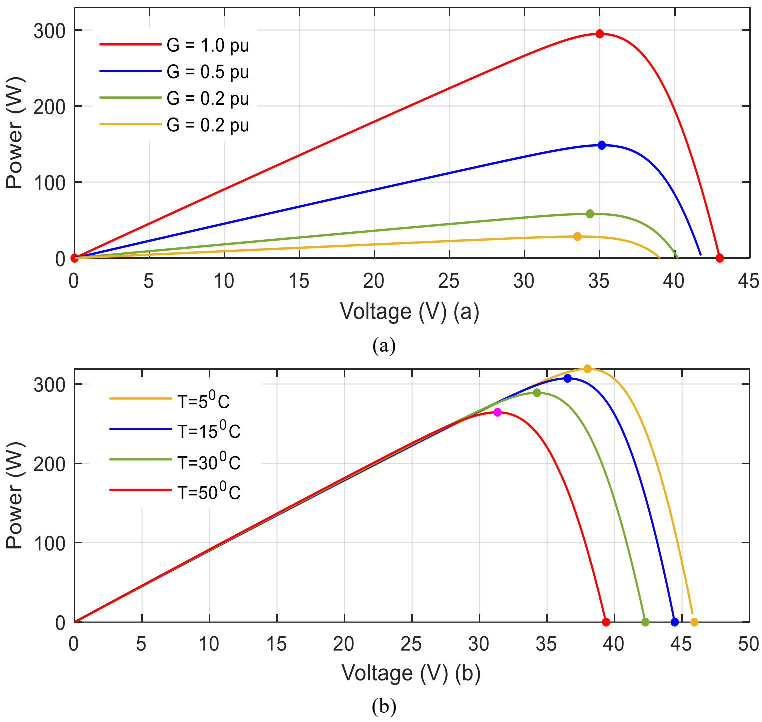

Fig. 2. (a) P-V curve for different values of irradiance, (b) P-V curve for different values of temperature. [Array type: Waaree Energies WSM-295; 1 series module; 1 parallel strings]

III. Bonobo Optimizer (BO) Algorithm

This article briefly overviews the Bonobo Optimizer (BO) algorithm, a newly created heuristic optimisation method. The algorithm is based on bonobos' social behaviour and reproduction strategies [18]. Bonobos, like many other primates, use a fission-fusion group strategy, dividing into smaller groups of varying sizes (fusion) and exploring their region independently as shown in Fig. 3. After that, they reintegrate (fusion) with the rest of society to engage in all the usual activities, such as sleeping with each other, Figurehting with competitors, and so on. In addition to these, bonobos use four distinct reproductive strategies: consortship mating, extra-group mating, restricted mating, and promiscuous mating. The underlying workings of various techniques are quite varied. The BO algorithm is developed by mathematically modelling them. According to the objective value, the alpha bonobo (α_{bonobo}) is called the best-rank bonobo in this method.

The BO algorithm first considers two separate phases, called positive and negative. Optimal living conditions, including enough of food and shelter, a high rate of successful mating, etc., characterise the positive phase. On the other hand, the negative phase is polar opposite to the positive one. The parameters positive phase count (PPC) and negative phase count (NPC) increase by one with each iteration, and the iteration moves through either a positive or negative phase. Nevertheless, when one of the parameters is raised, the other is initially set to 0.

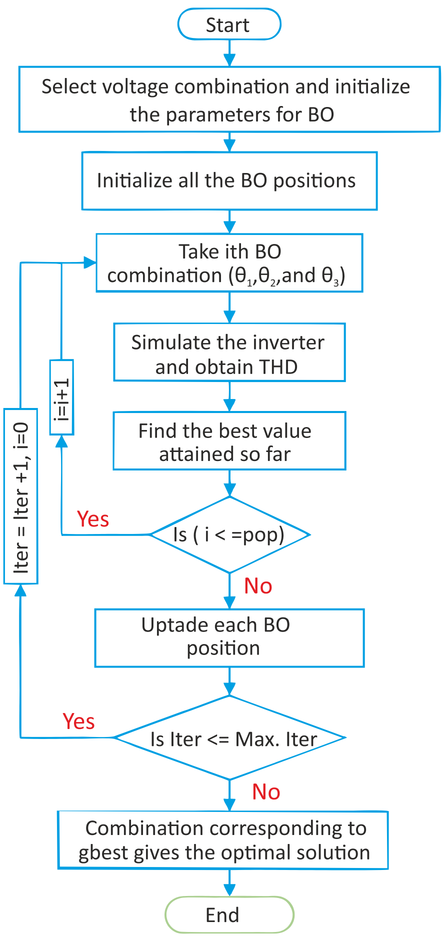

Fig. 3. Flow chart of the proposed strategy using BO

The largest size of a temporary sub-group ($tsgs_{max}$) is found by using Eq. (8) as a function of the total population size (N). The focal-fusion social strategy is used to choose which bonobos to mate with. The temporary sub-group size factor, denoted as tsgsfactor, determines the value of $tsgs_{max}$, which is maximum between 2 and ($tsg_{s_{factor}} \times N$).

$$tsgs\left(2, \left(tsg_{s_{\text{factor}}} \times N\right)\right)_{max} \tag{8}$$

At random, a size between 2 and $tsgs_{max}$ is chosen for the temporary subgroup. Then, out of all the bonobos in that subgroup, the one with the highest fitness value is chosen to mat, and that's when the process begins. Both restricted and promiscuous mating are more likely during the positive phase, but consortship and extra-group mating are more likely during the negative phase. In the BO algorithm, this likelihood is called the phase probability, or pp. By default, pp is set to 0.5 at the beginning. Nevertheless, this value is updated after each iteration based on the current phase and the number of phases. Its range during a positive phase is (0.5, 1.0), whereas during a negative phase it is (0, 0.5). Equation (9) provides the primary equation that governs a positive phase.

$$\begin{aligned} \text{new\_bonobo}_j = \ & \text{bonobo}_j^i \\ & + r_1 \times scab \\ & \times (\alpha_{\text{bonobo}}^j - \text{bonobo}_j^i) \\ & + (1 - r_1) \times scsb \\ & \times \text{flag} \times (\text{bonobo}_j^i \\ & - \text{bonobo}_j^p) \end{aligned} \tag{9}$$

$$\beta_1 = e^{(r_1^2 + r_1 - 2/r_1)} \tag{10}$$

$$\beta_2 = e^{(-r_1^2 + 2\times r_1 - 2/r_1)} \tag{11}$$

$$\begin{aligned} \text{new\_bonobo}_j = \ & \text{bonobo}_j^i \\ & + \beta_1 \\ & \times (\text{Var\_max}_j - \text{bonobo}_j^i) \end{aligned} \tag{12}$$

$$\begin{aligned} \text{new\_bonobo}_j = \ & \text{bonobo}_j^i \\ & - \beta_2 \\ & \times \left(\text{bonobo}_j^i - \text{Var\_}min_j\right) \end{aligned} \tag{13}$$

$$\begin{aligned} \text{new\_bonobo}_j = \ & \text{bonobo}_j^i \\ & - \beta_1 \\ & \times \left(\text{bonobo}_j^i - \text{Var\_}min_j\right) \end{aligned} \tag{14}$$

$$\begin{aligned} \text{new\_bonobo}_j = \ & \text{bonobo}_j^i \\ & + \beta_2 \\ & \times \left(\text{Var\_}max_j - \text{bonobo}_j^i\right) \end{aligned} \tag{15}$$

Here, α_{bonobo}^j and are variables for the alpha bonobo and its offspring, respectively, with j ranging from 1 to d, where d is the number of variables in the optimization problem. scab and scsb are sharing parameters, and the parameter flag is assigned as 1 or -1 based on a condition. In a negative phase, a new bonobo is generated during extra group mating by following the equations between (10) and (13).

In this case, β_1 and $\beta_2$are two intermediate variables, Var_{maxj} and Var_{minj} are the maximum and minimum values for the jth variable, and r is a random integer between zero and one. By collecting search-process data at each iteration's conclusion, we may adjust control parameters to focus on more fruitful areas of the variable space.

IV. PROPOSED STRATEGY

In Eq. (16), the fitness function (FF) is provided. Each term in the function f needs to equal zero in order to completely remove harmonics. The fitness function must satisfy the constraint given in equation (4).

$$f = \min_{\theta_i}\{|V_{1p} - V_{\text{ref}}| + (V_5)^2 + (V_7)^2\} = 0 \tag{16}$$

$$V_{\text{fund}} - V_{\text{ref}} \leq \varepsilon \tag{17}$$

V_{ref} is the desired reference voltage, and ε is the acceptable fault tolerance. ε = 2.2V (1% error) (218.8 and 222.2V) error can be considered as the solution for this study. The fundamental voltage is represented by the first term in the fitness function, while the second term represents the lower-order harmonics.

The proposed strategy for finding optimal switching angles using the BO algorithm is illustrated in Fig. 3. The voltage values of the V_{PV} panel are assumed to vary with a precision of 1V within the range of 105 volts to 115 volts. A total of 11 values within this range were considered, generating 1331 input data points. Subsequently, the BO algorithm was executed five times to calculate the switching angles θ_1, θ_2, and θ_3 corresponding to these input voltage values. The switching angles with the best fitness value were recorded in a table.

V. SIMULATION RESULTS

In a MATLAB/Simulink setting, the suggested strategy's simulation study was executed. We have created an m-file for the optimisation using BO after modelling a 7-level CHB in Simulink. Different combinations have been generated for this investigation by varying the voltages in increments of 1 V ([105, 105, 105], [105, 105, 106] ... [115, 115, 115]). Table 1 lists the parameters that were utilised by the BO algorithm. Table I presents the parameters employed in the BO algorithm, while Table II outlines the parameters utilized for the GA. Additionally, Table III provides an overview of the parameters applied in the PSO algorithm. Table IV displays the simulation results for 20 different voltage combinations that were created at random.

The findings show that BO alone yielded the lowest THD for every example, whereas the other methods produced higher THD values in most situations. Further, in contrast to other optimisation techniques, BO needs fewer iterations to discover the best solution, which is a crucial finding. While PSO and GA have required more iterations to obtain the globally optimum solution, BO only requires 12 iterations, as seen in Fig. 4.

This means that, compared to the other algorithms, BO reaches the global optimum far more quickly, as shown in the data above. It is possible to get trapped in the local optima of a certain algorithm due to the heuristic nature of all the algorithms used in this study.

However, the algorithms have been executed several times with the same input to check whether they converge to the global minimum. and, if so, to guarantee that they attain the global optimum. The output of this iterative process is shown in Table V. After feeding all the algorithms the identical input and running them for ten iterations in a row, we can determine how many function calls each algorithm needs to attain the specified global optimum. Also, this result shows that BO consistently got the same answer and uses far fewer function calls than the other methods. A computer with an Intel Core - i7 processor running at 5.0 GHz and 16 GB of RAM calculates the time needed for each BO function execution.

TABLE I. PARAMETERS USED FOR BO

Variable	Value
Probability of Phase (pp)	0.5
Directional Probability (pd)	0.5
Population size	50
Maximum iterations	100

TABLE II. PARAMETERS USED FOR GA

Variable	Value
Crossover probability	0.8
Mutation probability	0.2
Elitism probability	0.2
Population size	50
Maximum iterations	100

TABLE III. PARAMETERS USED FOR PSO

Variable	Value
Inertia Weight (w)	1.0
Inertia Weight Damping Ratio (wdamp)	0.99
Personal Learning Coefficient (c1)	1.50
Global Learning Coefficient (c2)	2.0
population size	50
Maximum iterations	100

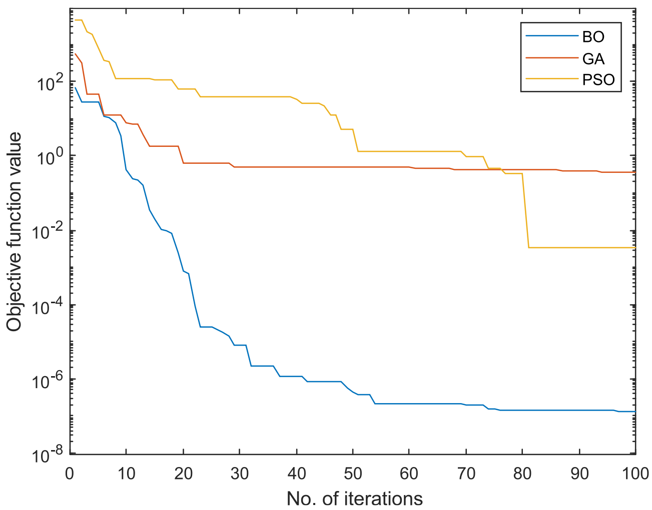

Fig. 4. Convergence rates of GA, PSO, and BO algorithms

TABLE IV. THE SWITCHING ANGLES AND SIMULATION RESULTS COMPUTED BY THE GA, PSO, AND BO ALGORITHMS FOR DIFFERENT VOLTAGE COMBINATIONS

S. No.	Voltages			BO			GA			PSO			%THD			%THDe			Vrms		
	V_{PV1}	V_{PV2}	V_{PV3}	θ_1	θ_2	θ_3	θ_1	θ_2	θ_3	θ_1	θ_2	θ_3	BO	GA	PSO	BO	GA	PSO	BO	GA	PSO
1	105	105	105	11.929	32.374	59.284	10.569	32.625	59.932	11.574	33.575	59.129	**6.91**	7.37	6.94	**0.03**	1.41	1.10	**220.1**	219.4	219.3
2	105	107	106	12.110	33.415	59.958	11.746	33.487	60.486	12.130	33.545	60.359	**6.66**	7.00	6.78	**0.03**	0.59	0.31	**220.0**	219.4	219.4
3	105	108	114	13.305	35.657	61.091	13.283	35.485	61.653	13.078	36.027	61.361	**7.15**	7.68	7.47	**0.03**	0.69	0.41	**220.1**	219.3	219.4
4	105	110	107	12.413	34.761	60.844	12.481	35.162	61.040	12.640	35.166	60.996	**6.99**	7.12	7.04	**0.03**	0.11	0.09	**220.1**	219.4	219.4
5	106	113	106	12.731	36.024	61.697	12.687	36.090	62.142	13.094	36.389	61.825	**7.74**	8.14	7.88	**0.03**	0.41	0.19	**220.0**	219.4	219.4
6	106	114	107	12.984	36.571	62.021	13.293	37.024	62.091	13.302	36.871	62.198	**8.14**	8.29	8.36	**0.02**	0.21	0.17	**220.0**	219.4	219.4
7	106	107	111	13.001	35.077	60.775	13.069	35.382	61.028	13.021	35.449	60.997	**6.80**	7.05	7.01	**0.03**	0.12	0.14	**220.1**	219.3	219.4
8	106	112	105	12.493	35.464	61.357	12.652	36.031	61.402	12.898	35.788	61.513	**7.39**	7.49	7.55	**0.04**	0.31	0.27	**220.1**	219.3	219.4
9	108	114	108	13.674	37.666	62.503	14.054	38.170	62.501	13.749	37.989	62.716	**8.77**	8.93	8.96	**0.02**	0.23	0.13	**220.1**	219.3	219.4
10	108	105	114	13.737	36.005	61.044	13.903	36.474	61.160	13.830	36.322	61.274	**7.17**	7.43	7.44	**0.04**	0.13	0.06	**220.0**	219.3	219.4
11	109	107	105	12.791	35.096	60.814	13.112	35.664	60.835	12.907	35.408	61.064	**6.81**	6.88	7.04	**0.03**	0.30	0.07	**220.1**	219.4	219.3
12	110	114	105	13.693	37.896	62.668	13.698	38.149	62.958	13.730	38.200	62.911	**8.86**	9.07	9.06	**0.04**	0.19	0.16	**220.1**	219.4	219.3
13	110	105	106	13.004	35.079	60.661	13.174	35.665	60.717	13.140	35.357	60.929	**6.67**	6.79	6.85	**0.04**	0.25	0.10	**220.0**	219.3	219.5
14	111	113	109	14.542	38.889	62.905	14.711	39.307	63.013	14.710	39.269	63.042	**9.29**	9.49	9.50	**0.05**	0.11	0.08	**220.1**	219.3	219.3
15	111	114	114	15.589	40.261	63.350	16.093	40.825	63.232	15.867	40.586	63.474	**10.25**	10.64	10.56	**0.04**	0.33	0.10	**220.1**	219.4	219.4
16	112	105	112	14.381	37.428	61.658	14.804	38.057	61.583	14.604	37.860	61.768	**8.12**	8.28	8.33	**0.05**	0.34	0.08	**220.1**	219.4	219.4
17	112	112	114	15.599	40.108	63.139	15.790	40.352	63.351	15.793	40.511	63.236	**10.08**	10.32	10.38	**0.03**	0.10	0.13	**220.1**	219.3	219.3
18	113	115	113	16.129	41.217	63.745	15.587	40.937	64.799	16.295	41.393	64.005	**11.04**	11.21	11.29	**0.04**	1.12	0.25	**220.1**	219.5	219.4
19	114	105	115	15.396	39.050	62.224	15.427	39.152	62.589	15.520	39.563	62.293	**9.13**	9.39	9.35	**0.05**	0.33	0.22	**220.1**	219.3	219.3
20	115	115	115	17.133	42.529	64.007	16.490	41.639	65.312	17.378	42.822	64.140	**11.77**	12.00	11.83	**0.03**	1.50	0.1	**220.0**	219.4	219.3

VI. Adaptive Switching Angle Strategy Utilizing Artificial Neural Networks (ANN)

The schematic representation of the proposed real-time algorithm, based on BO and artificial neural networks (ANN), is depicted in Fig. 8. For a 3-phase, 7-level inverter configure ration, optimal switching angles were pre-computed offline using the BO algorithm. This involved varying the panel voltage values (V_{PV_1}, V_{PV_2}, and V_{PV_3}) within the range of 105V to 115V with a precision of 1 volt to minimise THD. A lookup table was made to make implementation in real time easier by comparing all 113 (1331 possible combinations) with six different voltage changes for five panels. Table V provides a glimpse of a subsection of the dataset contained within the lookup table.

A tabular representation of the ANN's parameters may be seen in Table VII. The artificial neural network (ANN) was trained successfully using the generated data. The artificial neural network was trained by dividing the dataset into 70% training, 15% validation, and 15% testing. Following the successful training of the Artificial Neural Network (ANN) using the produced data, it has been included into the inverter system to calculate switching angles. The objective is to minimise the THDe and THD while keeping the fundamental voltage at a constant level. Table VIII shows the result of training the neural network. Fig. 9 shows the overlap between target and response variables and the coefficients of determination for the validation, training, and testing steps. R values are a statistical evaluation of how close the datasets are to the appropriate regression line. “Target” values displayed in regression charts represent “Measured” values, and “Output” values represent “Predicted” values. From the regression plot, the R values confirm the acceptable accuracies of the model in both the training and validation steps. As can be seen, in most cases, ANN could find values very close to the target values calculated by BO for the given input values.

TABLE V. Number of Function Calls to Reach the Optimum Value

Run Number	BO	GA	PSO
1	0.104	2.180	1.288
2	0.097	2.520	1.436
3	0.099	2.420	1.534
4	0.097	2.520	1.496
5	0.099	2.420	1.455
6	0.099	2.450	1.545
7	0.097	2.520	1.285
8	0.098	2.440	1.525
9	0.110	2.420	1.412
10	0.101	2.410	1.628
AVG	0.100	2.430	1.460

VII. Offline Simulation Results

BO algorithm was employed to calculate switching angles for 1331 different scenarios, and the results were stored in a table. Selected values from these calculations are presented in Table IV. Switching angles calculated using BO, GA, and PSO, along with root mean square (rms) value of the fundamental voltage, THD, and Eliminated THD (THDe) values, are presented in the same table for comparative analysis.

Tabular analysis reveals that the error in controlling the fundamental voltage for the BO algorithm is maximally 0.05%, whereas for the GA and PSO algorithms, it is 0.37%. The BO algorithm proves to be the most effective in suppressing selected harmonics. Regarding THDe, the PSO algorithm demonstrates superior performance compared to GA. Regarding THD, the BO algorithm consistently outperforms other algorithms in all scenarios, while GA and PSO occasionally surpass each other in certain instances. For the analysis given in Table IV, cases 1 as shown in Fig. 5, Fig. 6, and Fig. 7.

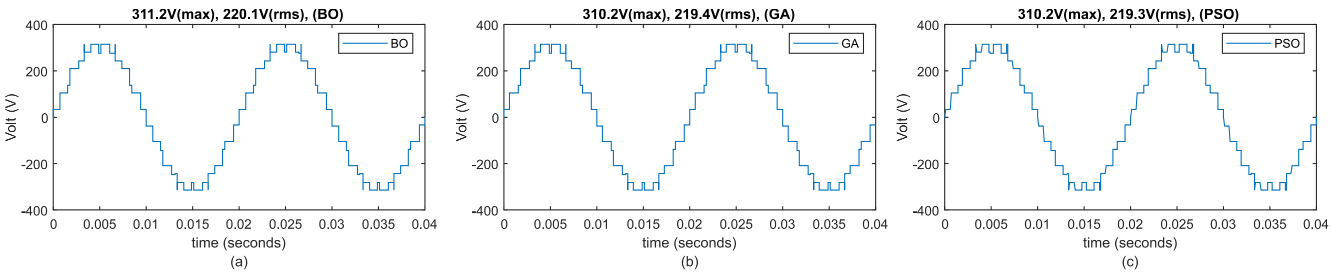

Fig. 5. Output voltage waveform for case 1 (a) BO, (b) GA, and (c) PSO

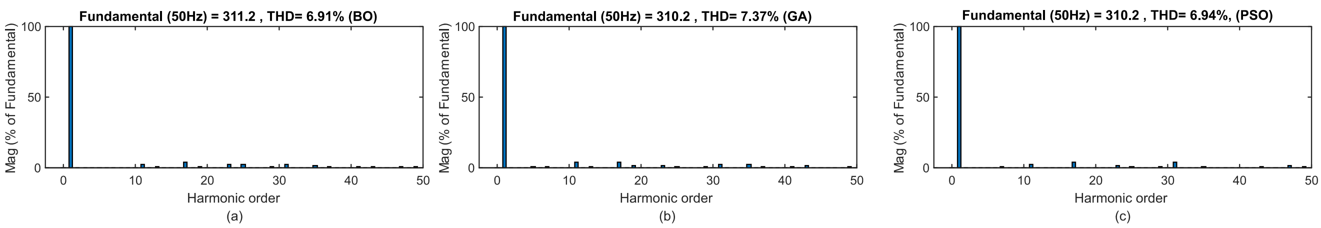

Fig. 6. THD spectrum for case 1: (a) BO, (b) GA, and (c) PSO

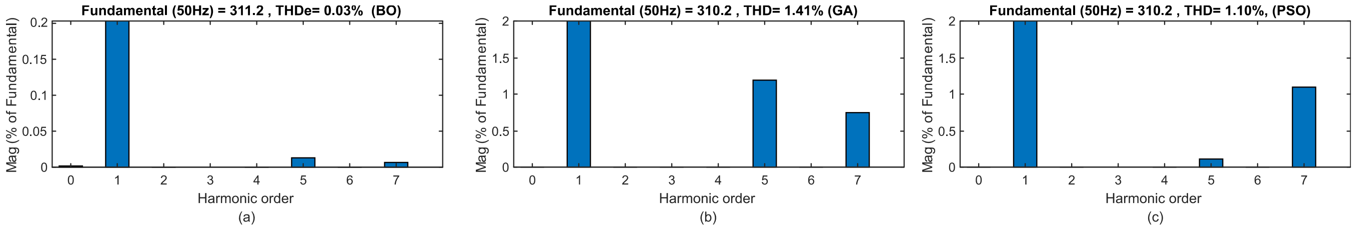

Fig. 7. THDe spectrum for case 1: (a) BO, (b) GA, and (c) PSO

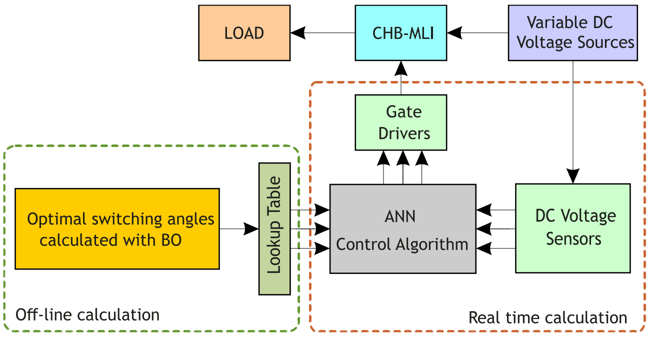

Fig. 8. Proposed strategy using ANN

Mean Square Error (MSE) represents the mean square difference between outputs and targets. If the MSE value is zero, it means there is no error. Therefore, it is a good result if the MSE value is close to zero. Regression (R) Values measure the correlation between outcomes and goals. Suppose the correlation value is 0.8<R<1, it can be interpreted that there is a very high correlation, and if R<0.2, there is a very weak correlation or no correlation. As evident, the MSE value is extremely close to zero, and the R-squared (R) values are 1. This implies that the data fitting is exact, and the model exhibits a high level of accuracy in capturing the underlying patterns in the data.

The ANN model has successfully computed the switching angles for all data points. A subset of these values is presented in Table IX. The switching angles provided in Table VI and Table IX were applied to the inverter in the MATLAB Simulink environment, and the simulation results are presented in Table X. As observed, the values calculated with BO closely resemble the real-time values as shown in Fig. 9.

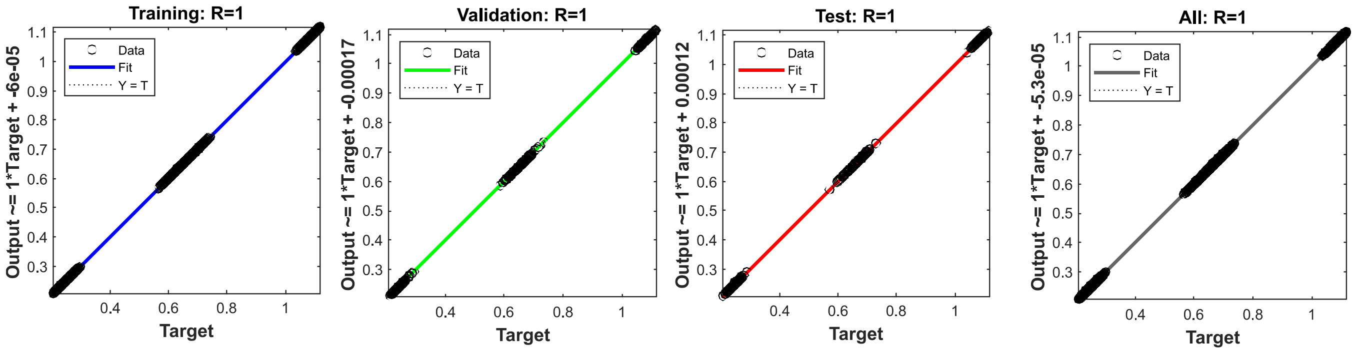

Fig. 9. Regression plot for training, test and validation of the ANN

TABLE VI. DATASET OBTAINED WITH BO

Input Voltages (V)	Output Angles (Degree)	Input Voltages (V)	Output Angles (Degree)
[V_1 V_2 V_3]	[θ_1 θ_2 θ_3]	[V_1 V_2 V_3]	[θ_1 θ_2 θ_3]
[105 105 105]	[11.929 32.374 59.284]	[110 105 115]	[14.374 37.179 61.526]
[105 105 106]	[12.043 32.624 59.424]	[110 108 113]	[14.374 37.732 61.987]
…	…	…	…
[106 105 105]	[12.095 32.878 59.549]	[111 113 105]	[13.847 38.023 62.642]
[106 107 109]	[12.714 34.609 60.558]	[111 114 114]	[15.589 40.261 63.350]
[106 114 105]	[12.661 36.135 61.841]	[111 115 113]	[15.540 40.342 63.483]
…	…	…	…
[107 105 111]	[13.072 34.822 60.524]	[112 105 105]	[13.298 35.801 61.011]
[107 107 108]	[12.787 34.850 60.679]	[112 112 112]	[15.230 39.675 63.042]
[107 109 115]	[14.051 37.142 61.792]	[112 115 105]	[14.353 39.075 63.248]
…	…	…	…
[108 105 108]	[12.861 34.590 60.419]	[113 106 115]	[15.259 38.910 62.250]
[108 111 109]	[13.523 36.921 61.925]	[113 107 114]	[15.211 39.007 62.376]
[108 114 114]	[14.734 38.951 62.896]	[114 108 113]	[15.434 39.562 62.662]
…	…	…	…
[109 111 107]	[13.449 36.928 61.959]	[114 105 105]	[13.759 36.752 61.448]
[109 112 108]	[13.719 37.473 62.262]	[115 115 114]	[16.931 42.316 63.990]
[109 114 114]	[15.016 39.387 63.055]	[115 115 115]	[17.133 42.529 64.007]

TABLE VII. NEURAL NETWORK PARAMETERS

Parameter	Value
Inputs	$[V_{dc1}, V_{dc2}, V_{dc3}]$
Outputs	$[\theta_1, \theta_2, \theta_3]$
No. of layers	3
Size of the hidden layers	10/10
Training data	216
Ratio of data (Training/testing/validation)	75/15/15
Training method	Trainlm (Back-propagation) Levenberg-Marquardt

TABLE VIII. MEAN SQUARED ERROR (MSE) AND REGRESSION (R) VALUES OF THE CREATED NEURAL NETWORK

	Samples	MSE	R
Training	5832	1.415e-07	1
Validation	1164	2.674e-07	1
Testing	1164	7.522e-07	1
All	7776	2.151e-07	1

TABLE IX. DATASET OBTAINED WITH BO-ANN

Input Voltages (V) [V_1 V_2 V_3]	Output Angles (Degree) [θ_1 θ_2 θ_3]	Input Voltages (V) [V_1 V_2 V_3]	Output Angles (Degree) [θ_1 θ_2 θ_3]
[105 105 105]	[11.882 32.355 59.329]	[110 105 115]	[14.349 37.186 61.516]
[105 105 106]	[12.029 32.640 59.458]	[110 108 113]	[14.383 37.748 61.995]
…	…	…	…
[106 105 105]	[12.103 32.887 59.576]	[111 113 105]	[13.830 38.011 62.656]
[106 107 109]	[12.707 34.600 60.565]	[111 114 114]	[15.585 40.256 63.354]
[106 114 105]	[12.658 36.118 61.854]	[111 115 113]	[15.524 40.336 63.475]
…	…	…	…
[107 105 111]	[13.071 34.814 60.525]	[112 105 105]	[13.291 35.833 61.012]
[107 107 108]	[12.782 34.849 60.687]	[112 112 112]	[15.259 39.701 63.060]
[107 109 115]	[14.019 37.108 61.784]	[112 115 105]	[14.396 39.076 63.230]
…	…	…	…
[108 105 108]	[12.858 34.570 60.423]	[113 106 115]	[15.239 38.929 62.249]
[108 111 109]	[13.520 36.921 61.931]	[113 107 114]	[15.188 39.028 62.372]
[108 114 114]	[14.711 38.968 62.894]	[114 108 113]	[15.450 39.595 62.661]
…	…	…	…
[109 111 107]	[13.439 36.907 61.965]	[114 105 105]	[13.733 36.730 61.452]
[109 112 108]	[13.706 37.457 62.268]	[115 115 114]	[16.944 42.315 64.015]
[109 114 114]	[14.999 39.395 63.056]	[115 115 115]	[17.147 42.535 64.053]

VIII. REAL-TIME SIMULATION RESULTS

A closed-loop simulation has been created in the MATLAB program to test the effectiveness of the BO-ANN algorithm. Real-time application has been implemented for the Scenario 1: DC sources have been used as input voltage sources. The voltage values of DC sources can vary as both integers and fractions. The range of variations, input voltage values, and switching angles calculated with BO-ANN for Scenario 1 are provided in Table XI. The input voltages and switching angles provided for Scenario 1 have been applied to the inverter. Simulation results are presented in Table XII. As observed, the selected harmonics have been effectively suppressed by controlling the fundamental voltage with a slight error of approximately 0.05%. Detailed explanations for each scenario are provided below. The waveform of the inverter output voltage for these angles is shown in Fig. 10(a). Fig. 10(b) presents the variation graph of the rms value of the load voltage. After a small fluctuation at the time instants of 0.1, 0.2, 0.3, and 0.4, seconds, the fundamental voltage is rapidly controlled. For Scenario 1, the load voltage waveform is presented in Fig. 11, while the THD and THDe values are depicted in Fig. 12 and Fig. 13, respectively.

Case 1: For the time interval between 0.0 and 0.1 seconds, the input voltages are $V_{DC_1} = 105V, V_{DC_2} = 106V, and\ V_{DC_3} = 107V$. In this case, the switching angles are calculated as $\theta_1 = 12.179, \theta_2 = 33.257, and\ \theta_3 = 59.828$. As seen, the maximum value of the load voltage Van is 311.3V, while the rms value is obtained as 220.1V in Fig. 11(a). The fundamental voltage is controlled at a rate of 0.05%. Fig. 12(a) presents the THD value of 6.63%. As shown in Fig. 13(a), the THDe value is obtained as 0.02%, and the selected harmonics are 5th =0.01% and 7th =0.02%.

Case 2: For the time interval between 0.1 and 0.2 seconds, the input voltages are $V_{DC_1} = 114V, V_{DC_2} = 105V, and\ V_{DC_3} = 109V$. In this case, the switching angles are calculated as $\theta_1 = 14.414, \theta_2 = 37.667, and\ \theta_3 = 61.822$. As seen, the maximum value of the load voltage Van is 311.2V, while the rms value is obtained as 220.1V in Fig. 11(b). The fundamental voltage is controlled at a rate of 0.05%. Fig. 12(b) presents the THD value of 8.25%. As shown in Fig. 13(b), the THDe value is obtained as 0.07%, and the selected harmonics are 5th =0.05% and 7th =0.04%.

Case 3: For the time interval between 0.2 and 0.3 seconds, the input voltages are $V_{DC_1} = 105.25V, V_{DC_2} = 111.55V, and\ V_{DC_3} = 114.85V$. In this case, the switching angles are calculated as $\theta_1 = 13.964, \theta_2 = 37.509, and\ \theta_3 = 62.187$. As seen, the maximum value of the load voltage Van is 311.3V, while the rms value is obtained as 220.1V in Fig. 11(c). The fundamental voltage is controlled at a rate of 0.05%. Fig. 12(c) presents the THD value of 8.61%. As shown in Fig. 13(c), the THDe value is obtained as 0.04%, and the selected harmonics are 5th =0.03% and 7th =0.02%.

Case 4: For the time interval between 0.3 and 0.4 seconds, the input voltages are $V_{DC_1} = 107.18V, V_{DC_2} = 111.45V, and\ V_{DC_3} = 107.55V$. In this case, the switching angles are calculated as $\theta_1 = 13.125, \theta_2 = 36.381, and\ \theta_3 = 61.739$. As seen, the maximum value of the load voltage Van is 311.3V, while the rms value is obtained as 220.1V in Fig. 11(d). The fundamental voltage is controlled at a rate of 0.05%. Fig. 12(d) presents the THD value of 7.80%. As shown in Fig. 13(d), the THDe value is obtained as 0.03%, and the selected harmonics are 5th =0.01% and 7th =0.02%.

TABLE X. SIMULATION RESULTS CALCULATED WITH BO AND BO-ANN

Input Voltages (V)	%THD		%THDe		Vrms		error		Input Voltages (V)	%THD		%THDe		Vrms		Error	
[V₁ V₂ V₃]	BO	BO-ANN	BO	BO-ANN	BO	BO-ANN	BO	BO-ANN	[V₁ V₂ V₃]	BO	BO-ANN	BO	BO-ANN	BO	BO-ANN	BO	BO-ANN
[105 105 105]	6.91	6.92	0.03	0.04	220.1	220.0	0.05	0.00	[110 105 115]	7.99	7.98	0.02	0.05	220.1	220.0	0.05	0.00
[105 105 106]	6.79	6.78	0.02	0.05	220.1	220.0	0.05	0.00	[110 108 113]	8.47	8.47	0.02	0.04	220.1	220.1	0.05	0.00
…									…								
[106 105 105]	6.67	6.69	0.03	0.02	220.1	220.0	0.05	0.00	[111 113 105]	8.87	8.87	0.02	0.02	220.0	220.0	0.00	0.00
[106 107 109]	6.66	6.66	0.04	0.04	220.1	220.1	0.05	0.05	[111 114 114]	10.25	10.26	0.04	0.05	220.1	220.1	0.05	0.05
[106 114 105]	7.90	7.88	0.02	0.04	220.0	220.1	0.00	0.05	[111 115 113]	10.34	10.32	0.04	0.04	220.0	220.1	0.00	0.05
…									…								
[107 105 111]	6.59	6.59	0.03	0.03	220.1	220.1	0.05	0.05	[112 105 105]	6.99	7.00	0.04	0.06	220.2	220.1	0.09	0.05
[107 107 108]	6.73	6.73	0.04	0.04	220.1	220.1	0.05	0.05	[112 112 112]	9.76	9.77	0.03	0.03	220.1	220.0	0.05	0.05
[107 109 115]	8.21	8.19	0.02	0.04	220.1	220.1	0.05	0.05	[112 115 105]	9.43	9.44	0.03	0.02	220.1	220.1	0.05	0.05
…									…								
[108 105 108]	6.53	6.55	0.03	0.04	220.1	220.1	0.05	0.05	[113 106 115]	9.06	9.07	0.03	0.04	220.1	220.1	0.05	0.05
[108 111 109]	8.16	8.16	0.04	0.04	220.1	220.1	0.05	0.05	[113 107 114]	9.17	9.16	0.05	0.03	220.0	220.0	0.00	0.00
[108 114 114]	9.43	9.41	0.04	0.03	220.1	220.1	0.05	0.05	[114 108 113]	9.52	9.55	0.02	0.05	220.0	220.1	0.00	0.05
…									…								
[109 111 107]	8.14	8.15	0.03	0.05	220.0	220.1	0.00	0.05	[114 105 105]	7.62	7.61	0.04	0.05	220.1	220.1	0.05	0.05
[109 112 108]	8.51	8.52	0.03	0.04	220.0	220.1	0.00	0.04	[115 115 114]	11.72	11.73	0.05	0.04	220.1	220.0	0.05	0.00
[109 114 114]	9.66	9.66	0.02	0.06	220.1	220.1	0.05	0.05	[115 115 115]	11.77	11.78	0.03	0.05	220.0	220.0	0.00	0.00

TABLE XI. SWITCHING ANGLES VERSUS DC VOLTAGES FOR SCENARIO 1

Case	Input Voltage			Switching Angles (degree)		
	V_{DC1}	V_{DC2}	V_{DC3}	θ_1	θ_2	θ_3
0.0s< t<0.1s	105.00	106.00	107.00	12.179	33.257	59.828
0.1s≤ t <0.2s	114.00	105.00	109.00	14.414	37.667	61.822
0.2s≤ t <0.3s	105.25	112.55	114.85	13.964	37.509	62.187
0.3s≤ t <0.4s	107.18	111.45	107.55	13.125	36.381	61.739

TABLE XII. HARMONIC ANALYSIS RESULTS FOR SCENARIO-1

Case	Line Voltage		Load Voltage				Harmonic order (%)	
	V_{ab}(max)	V_{ab}(rms)	Van(max)	Van(rms)	THD	THDe	5^{th}	7^{th}
0.0s< t <0.1s	539.1	381.2	311.3	220.1	6.63	**0.02**	**0.01**	**0.02**
0.1s< t <0.2s	539.0	381.2	311.2	220.1	8.25	**0.07**	**0.05**	**0.04**
0.2s< t <0.3s	539.1	381.2	311.3	220.1	8.61	**0.04**	**0.03**	**0.02**
0.3s< t <0.4s	539.2	381. 3	311.3	220.1	7.80	**0.03**	**0.01**	**0.02**

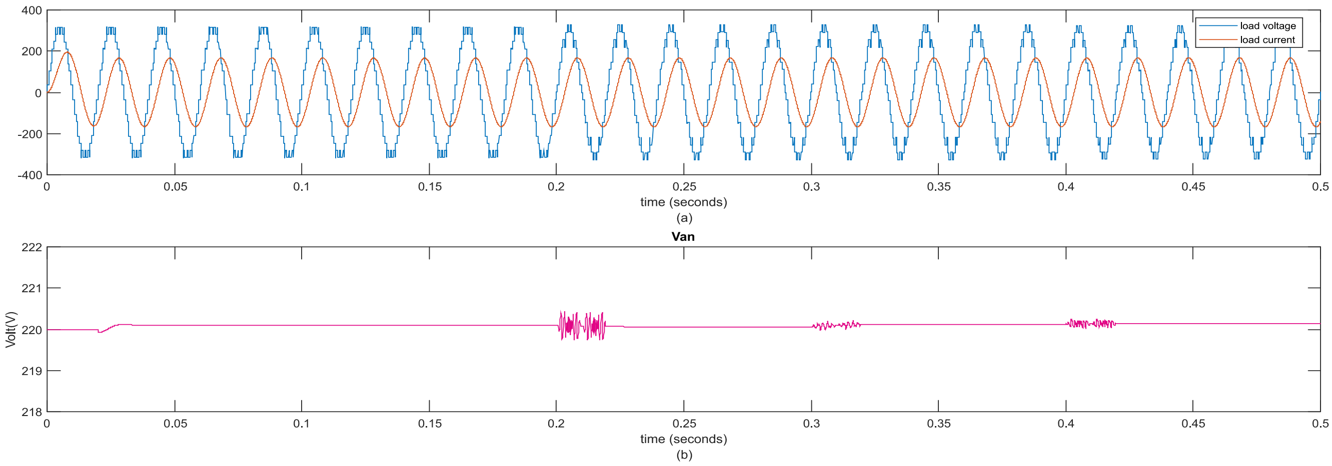

Fig. 10. During scenario 1 (a) inverter load voltage and current waveform (b) Van rms change graph

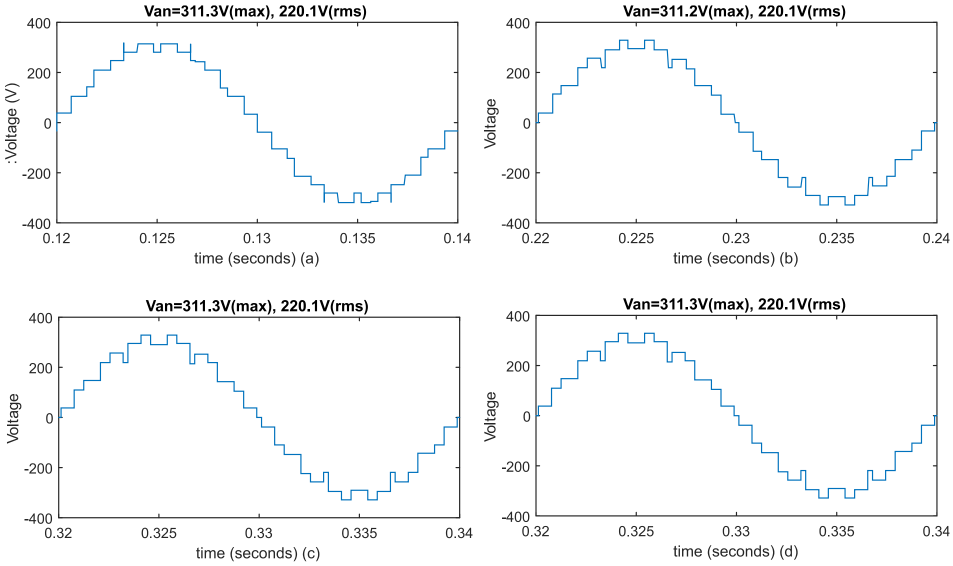

Fig. 11. Load voltage waveforms (Van) for Scenario -1 (a) case 1, (b) case 2, (c) case 3, (d) case 4

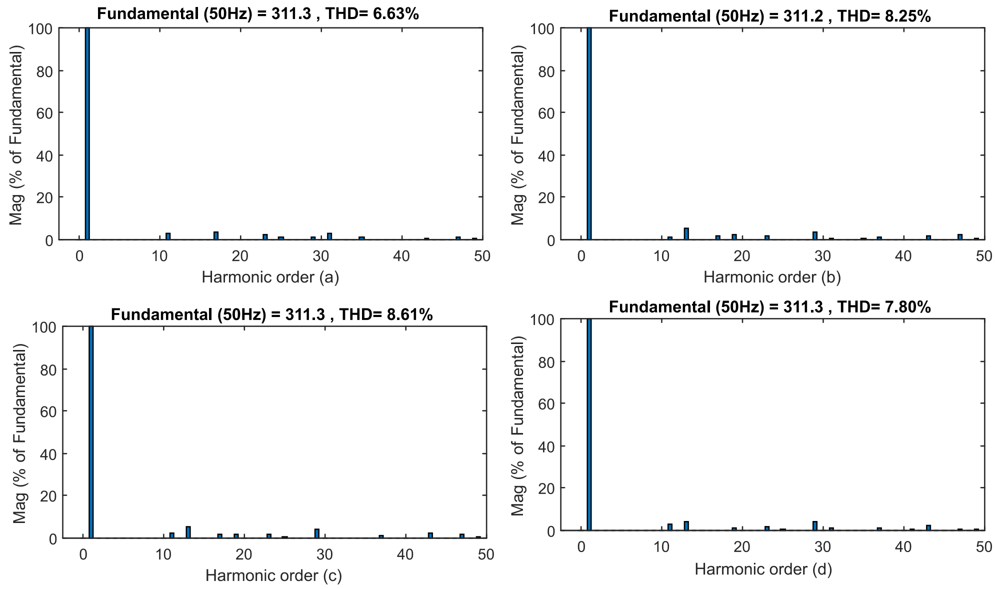

Fig. 12. Harmonic analysis for Van (Scenario-1) (THD) (a) case 1, (b) case 2, (c) case 3, d) case 4

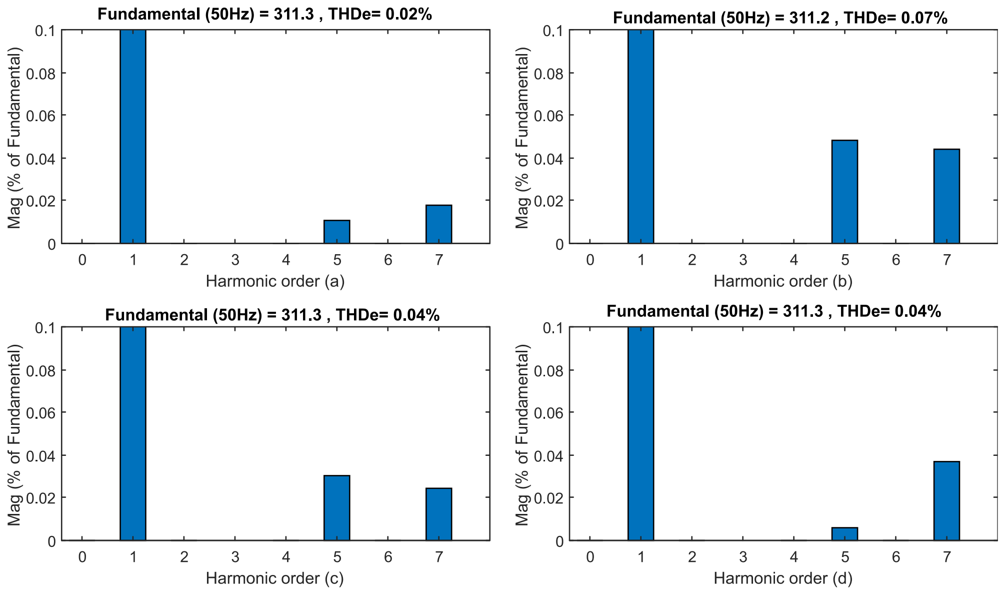

Fig. 13. Harmonic analysis for Van (Scenario-1) (THDe) (a) case 1, (b) case 2, (c) case 3, d) case 4

IX. CONCLUSION

In the pursuit of enhanced power quality, the reduction of harmonics in multi-level inverters emerges as a pivotal consideration. While the Sinusoidal Pulse Width Modulation (SHE-PWM) method commonly addresses lower-order harmonics under uniform DC supply conditions, the challenge persists when confronting uneven DC sources in Cascade H-Bridge (CHB) configurations. In response, our study proposes a novel strategy employing Binary Optimization (BO) as the core optimization framework, aimed at minimizing total harmonic distortion (THD).

Validated through rigorous simulations on a Simulink model and seamlessly integrated into practical implementations, our proposed approach stands as a robust solution. A noteworthy facet of our methodology involves the utilization of an Artificial Neural Network (ANN) to discern optimal firing angles, ensuring real-time adaptability and responsiveness. This pivotal adaptation renders our technique particularly apt for applications reliant on Photovoltaic (PV)-based CHB-Multi-Level Inverters (MLI).

Looking forward, the scalability and adaptability of our technique underscore its potential for broader real-world deployment. Moreover, our study sets the stage for future explorations into advanced optimization algorithms, adaptive control paradigms, and the seamless integration of emerging technologies. By addressing these facets, we aim to catalyze continued advancements in the domain of multi-level inverter design and power quality enhancement, thereby driving innovation and fostering sustainable progress.

REFERENCES

[1] R. Portillo, L. G. Franquelo, J. Napoles, J. I. Leon, and M. A. Aguirre, "Selective harmonic elimination technique for high power converters," *IEEE Trans. Ind. Electron.*, vol. 57, pp. 2315–2323, 2010.

[2] J. Kumar, "THD analysis for different levels of cascade multilevel inverters for industrial applications," *Int. J. Emerging Technol. Adv. Eng.*, vol. 2, pp. 237–244, 2012.

[3] J. N. Chiasson, L. M. Tolbert, K. J. McKenzie, and Z. Du, "Elimination of harmonics in a multilevel converter using the theory of symmetric polynomials and resultants," *IEEE Trans. Control Syst. Technol.*, vol. 13, pp. 216–223, 2005.

[4] M. Vesapogu, S. Peddakotla, and S. R. A. Kuppa, "Harmonic analysis and FPGA implementation of SHE controlled three-phase CHB 11-level inverter in MV drives using deterministic and stochastic optimization techniques," *Springer Plus*, vol. 2, p. 370, 2013.

[5] M. Aleenejad, R. Ahmadi, and P. Moamaei, "Selective harmonic elimination for cascaded multicell multilevel power converters with a higher number of H-bridge modules," in *2014 Power and Energy Conference at Illinois (PECI)*, pp. 1–5, 2014.

[6] B. Ozpineci, L. M. Tolbert, and J. N. Chiasson, "Harmonic optimization of multilevel converters using genetic algorithms," in *Power Electronics Specialists Conference, 2004. PESC 04. 2004 IEEE 35th Annual*, vol. 5, 3911–3916, 2004.

[7] K. Haghdar, H. A. Shayanfar, and M. H. Shahidi Alavi, "Selective harmonics elimination of multi-level inverters via methods of GPS, SA, and GA," in *Power and Energy Engineering Conference (APPEEC)*, pp. 1–5, 2011.

[8] Y. Bektaş and H. Karaca, "Red deer algorithm-based selective harmonic elimination for renewable energy application with unequal DC sources," *Energy Reports*, vol. 8, pp. 588-596, 2022.

[9] Y. Bektaş, H. Karaca, T. A. Taha, and H. I. Zaynal, "Red deer algorithm-based selective harmonic elimination technique for multilevel inverters," *Bulletin of Electrical Engineering and Informatics*, vol. 12, no. 5, pp. 2643-2650, 2023.

[10] Y. Bektaş and H. Karaca, "Red deer algorithm-based harmonic mitigation for asymmetric cascaded multilevel inverters," in *2022 57th International Scientific Conference on Information, Communication and Energy Systems and Technologies (ICEST)*, pp. 1-4, 2022.

[11] P. Gaur, Y. P. Verma, and P. Singh, "A particle swarm optimization-based switching scheme for seven-level cascaded hybrid bridge inverter," *Proceeding of International Conference on Intelligent Communication, Control and Devices: ICICCD 2016*, pp. 609–615, 2017.

[12] Y. Xin, J. Yi, K. Zhang, C. Chen, and J. Xiong, "Offline selective harmonic elimination with (2N+1) output voltage levels in modular multilevel converter using a differential harmony search algorithm," *IEEE Access*, vol. 8, pp. 121596-121610, 2020.

[13] J. Kumar, J. Gambhir, and A. Kumar, "Control of switching angles for a CMLI using ANN," in *Recent Advances in Engineering and Computational Sciences (RAECS)*, vol. 2014, pp. 1–6, 2014.

[14] C. Buccella, M. G. Cimoroni, H. Latafat, G. Graditi, and R. Yang, "Selective harmonic elimination in a seven-level cascaded multilevel inverter based on graphical analysis," in *IECON 2016-42nd Annual Conference of the IEEE Industrial Electronics Society*, pp. 2563–2568, Oct 2016.

[15] K. Yang, X. Tang, Q. Zhang, and W. Yu, "Unified selective harmonic elimination for fundamental frequency modulated multilevel converter with unequal DC levels," in *IECON 2016-42nd Annual Conference of the IEEE Industrial Electronics Society*, pp. 3623–3628, Oct 2016.

[16] M. Hajizadeh and S. H. Fathi, "Selective harmonic elimination strategy for cascaded H-bridge five-level inverter with arbitrary power sharing among the cells," *IET Power Electron*, vol. 9, pp. 95–101, 2016.

[17] M. S. A. Dahidah, G. Konstantinou, and V. G. Agelidis, "A review of multilevel selective harmonic elimination PWM: Formulations, solving algorithms, implementation, and applications," *IEEE Trans. Power Electron.*, vol. 30, pp. 4091–4106, 2015.

[18] A. K. Das and D. K. Pratihar, "A new bonobo optimizer (BO) for real-parameter optimization," in *2019 IEEE Region 10 Symposium (TENSYMP)*, pp. 108-113, 2019.

[19] J. H. Almazán-Covarrubias, H. Peraza-Vázquez, A. F. Peña-Delgado, and P. M. García-Vite, "An improved Dingo optimization algorithm applied to SHE-PWM modulation strategy," *Applied Sciences*, vol. 12, no. 3, p. 992, 2022.

[20] P. Kumar Kar, A. Priyadarshi, and S. Bhaskar Karanki, "Selective harmonics elimination using whale optimisation algorithm for a single-phase-modified source switched multilevel inverter," *IET Power Electronics*, vol. 12, no. 8, pp. 1952-1963, 2019.

[21] A. Routray, R. K. Singh, and R. Mahanty, "Harmonic reduction in hybrid cascaded multilevel inverter using modified grey wolf optimization," *IEEE Transactions on Industry Applications*, vol. 56, no. 2, pp. 1827-1838, 2019.

[22] A. F. Peña-Delgado *et al*., "A novel bio-inspired algorithm applied to selective harmonic elimination in a three-phase eleven-level inverter," *Mathematical Problems in Engineering*, vol. 2020, pp. 1-10, 2020.

[23] S. S. Kumar, M. W. Iruthayarajan, and T. Sivakumar, "Evolutionary algorithm based selective harmonic elimination for three-phase cascaded H-bridge multilevel inverters with optimized input sources," *Journal of Power Electronics*, vol. 20, pp. 1172-1183, 2020.

[24] S. Kundu, A. D. Burman, S. K. Giri, S. Mukherjee, and S. Banerjee, "Comparative study between different optimisation techniques for finding precise switching angle for SHE-PWM of three-phase seven-level cascaded H-bridge inverter," *IET Power Electronics*, vol. 11, no. 3, pp. 600-609, 2018.

[25] M. Saglam, Y. Bektas, and O. A. Karaman, "Dandelion Optimizer and Gold Rush Optimizer Algorithm-Based Optimization of Multilevel Inverters," *Arabian Journal for Science and Engineering*, pp. 1-24, 2024.

[26] M. G. Sundari, M. Rajaram, and S. Balaraman, "Application of improved firefly algorithm for programmed PWM in multilevel inverter with adjustable DC sources," *Applied soft computing*, vol. 41, pp. 169-179, 2016.

[27] A. Hassan, X. Yang, W. Chen, and M. A. Houran, "A state of the art of the multilevel inverters with reduced count components," *Electronics*, vol. 9, no. 11, p. 1924, 2022.

[28] S. Choudhury, M. Bajaj, T. Dash, S. Kamel, and F. Jurado, "Multilevel inverter: A survey on classical and advanced topologies, control

schemes, applications to power system and future prospects," *Energies*, vol. 14, no. 18, p. 5773, 2021.

[29] G. K. Srinivasan, M. Rivera, V. Loganathan, D. Ravikumar, and B. Mohan, "Trends and challenges in multi-level inverter with reduced switches," *Electronics*, vol. 10, no. 4, p. 368, 2021.

[30] Z. B. Duranay and H. Guldemir, "Extreme learning machine based selected harmonic elimination for single phase inverters," *Measurement*, vol. 131, pp. 300-308, 2019.

[31] M. Ahmed, A. Sheir, and M. Orabi, "Real-time solution and implementation of selective harmonic elimination of seven-level multilevel inverter," *IEEE Journal of Emerging and Selected Topics in Power Electronics*, vol. 5, no. 4, pp. 1700-1709, 2017.

[32] A. Marquez Alcaide *et al*., "Real-time selective harmonic mitigation technique for power converters based on the exchange market algorithm," *Energies*, vol. 13, no. 7, p. 1659, 2020.

[33] M. Al-Hitmi, S. Ahmad, A. Iqbal, S. Padmanaban, and I. Ashraf, "Selective harmonic elimination in a wide modulation range using modified Newton–Raphson and pattern generation methods for a multilevel inverter," *Energies*, vol. 11, no. 2, p. 458, 2018.

[34] A. F. Peña-Delgado *et al*., "A novel bio-inspired algorithm applied to selective harmonic elimination in a three-phase eleven-level inverter," *Mathematical Problems in Engineering*, vol. 2020, pp. 1-10, 2020.

[35] H. Juma'a and T. Atyia, "Design and Implementation of multi-level inverter for PV system with various DC Sources," *NTU Journal of Renewable Energy*, vol. 5, no. 1, pp. 24-33, 2023.

[36] T. A. Taha, M. K. Hassan, H. I. Zaynal, and N. I. A. Wahab, "Big Data for Smart Grid: A Case Study," in *Big Data Analytics Framework for Smart Grids*, pp. 142-180, 2024.

[37] Z. Ali, Z. M. Abdullah, B. A. Naser, R. W. Daoud, and A. H. Ahmed, "Design of a Single-Phase Inverter for Solar Energy Conversion System," *NTU Journal of Renewable Energy*, vol. 1, no. 1, pp. 38-42, 2021.

[38] E. H. I. Albajari and S. R. Aslan, "Exploring the Synergy of Integration: Assessing the Performance of Hydraulic Storage and Solar Power Integration in Kirkuk city," *NTU Journal of Renewable Energy*, vol. 5, no. 1, pp. 1-7, 2023.

[39] M. R. J. Oskuee, M. Karimi, S. N. Ravadanegh, and G. B. Gharehpetian, "An innovative scheme of symmetric multilevel voltage source inverter with lower number of circuit devices," *IEEE Trans on Industrial Electronics*, vol. 62, pp. 6965-6973, 2015.

[40] E. Babaei, S. Laali, and Z. Bayat, "A single-phase cascaded multilevel inverter based on a new basic unit with reduced number of power switches," *IEEE Trans on Industrial Electronics*, vol. 62, pp. 922-929, 2015.

[41] T. A. Taha, A. S. T. Hussain, and K. A. Taha, "Design solar thermal energy harvesting system, in *AIP Conference Proceedings*, vol. 2591, no. 1, 2023.

[42] A. K. Gupta and A. M. Khambadkone, "A space vector PWM scheme for multilevel inverters based on two-level space vector PWM," *IEEE Trans on Industrial Electronics*, vol. 53, pp. 1631-1639, 2006.

[43] J. R. Wells, X. Geng, P. L. Chapman, P. L. Krein, and B. M. Nee, "Modulation-based harmonic elimination," *IEEE Trans on Power Electronics*, vol. 22, pp. 336-340, 2007.

[44] K. Yang, Q. Zhang, R. Yuan, W. Yu, J. Yuan, and J. Wang, "Selective harmonic elimination with groebner bases and symmetric polynominals," *IEEE Trans on Power Electronics*, vol. 31, pp. 2742-2752, 2016.

[45] H. I. Zaynal, A. S. T. Hussain, T. A. Taha, A. A. Yass, S. R. Ahmed, and S. A. Ahmed, "High Pressure Water Solar Collector as Potential of Mini Steam Power Plant in Iraq," in *2023 7th International Symposium on Innovative Approaches in Smart Technologies (ISAS)*, pp. 1-9, 2023.

[46] J. N. Chiasson, L. M. Tolbert, K. Z. McKenzie, and Z. Du, "A unified approach to solving the harmonic equations in multilevel inverters," *IEEE Trans on Power Electronics*, vol. 19, pp. 478-790, 2004.

[47] S. Debnanth and R. N. Ray, "Harmonic elimination in multilevel inverter using GA and PSO; a comparison," *Proceedings of 2012 IEEE Students' Conference on Electrical, Electronics and Computer Science*, pp. 1-5, 2012.

[48] A. S. T. Hussain, D. Z. Ghafoor, S. A. Ahmed, and T. A. Taha, "Smart inverter for low power application based hybrid power system," in *AIP Conference Proceedings*, vol. 2787, no. 1, 2023.

[49] M. H. Etesami, N. Farokhnia, and S. H. Fathi, "Colonial competitive algorithm development toward harmonic minimization in multilevel inverters," *IEEE Trans on Industrial Informatics*, vol. 11, pp. 459-466, 2015.

[50] O. Bouhali, F. Bouaziz, N. Rizoug, and A. Talha, "Solving harmonics elimination equations in multi-level inverters by using neural networks," *International Journal of Information and Engineering*, vol. 3, pp. 191-195, 2013.

[51] J. Xue and B. Shen, "Dung beetle optimizer:a new meta-heuristic algorithm for global optimization," *The Journal of Supercomputing*, vol. 79, pp. 7305-7336, 2023.

[52] X. Zhu, C. Ni, G. Chen, and J. Guo, "Optimization of tungsten heavy alloy cutting parameters based on RSM and reinforcement dung beetle algorithm," *Sensors*, vol. 23, pp. 5616-5629, 2023.

[53] E. Bektaş, K. C. Bayındır, and H. Karaca, "A new bridgeless multilevel inverter reduced number of power switches structure with reduced number of power switches," *Proceedings of ELECO 2017 10th International Conference on Electrical and Electronics Engineering*, pp. 300-304, 2017.

[54] M. A. Memon, M. D. Siddique, S. Mekhilef, M. Mubin, "Asynchorus particle swarm optimization-genetic algorithm (APSO-GA) based selective harmonic elimination in cascaded H-Bridge multilevel inverter," *IEEE Transactions on Industrial Electronics*, vol. 69, no. 2, pp. 1477-1487, 2022.

[55] F. H. Meria, S. Algburi, and O. K. Ahmed, "Impact of porous media on PV/thermal system performance: A short review," *Energy Reports*, vol. 11, pp. 1803-1819, 2024.

[56] S. Algburi, O. K. Ahmed, A. A. Abdullah, and F. S. Atallah, "Comparative assessment of PV/Trombe wall performance: Compound influence of paraffin wax and reflective mirrors," *Results in Engineering*, vol. 20, p. 101433, 2023.

[57] A. A. Badr, O. K. Ahmed, and O. R. Alomar, "Performance of solar vortex engine integrated with the PV panel: Experimental assessment," *Renewable Energy*, vol. 216, p. 119073, 2023.

[58] A. E. Ibrahim, N. M. Nor, I. B. M. Nawi, M. F. Ramlie, and K. N. Mohdhasan, "Genetic algorithm to improve power output of photovoltaic system under partial shaded condition," *International Journal of Power Electronics and Drive System (IJPEDS)*, vol. 10, pp. 2182-2189, 2019.

[59] M. Sadoughi, A. Pourdadashnia, M. F. Kangarlu, and S. Galvani, "PSO-optimized SHE-PWM technique in a cascaded H-Bridge multilevel inverter for variable output voltage applications," *IEEE Transactions on Power Electronics*, vol. 37, no. 7, pp. 8065-8075, 2022.

[60] M. A. Hoque, M. K. Hassan, A. Hajjo, and T. A. Taha, "Investigation of Battery Energy Storage System (BESS) during Loading Variation," *Journal of Advanced Research in Applied Mechanics*, vol. 110, no. 1, pp. 86-96, 2023.

[61] B. Ozpineci, L. M. Tolbert, and J. N. Chiasson, "Harmonic optimization of multilevel converters using genetic algorithms," *IEEE Power Electronics Letters*, vol. 3, no. 3, pp. 92–95, 2005.

[62] J. Chiasson, L. Tolbert, K. McKenzie, and Z. Du, "Eliminating harmonics in a multilevel converter using resultant theory," in *Power Electronics Specialists Conference*, vol. 2, pp. 503–508, 2002.

[63] T. A. Taha, H. I. Zaynal, A. S. T. Hussain, H. Desa, and F. H. Taha, "Definite time over-current protection on transmission line using MATLAB/Simulink," *Bulletin of Electrical Engineering and Informatics*, vol. 13, no. 2, pp. 713-723, 2024.

[64] R. M. Hossam, G. M. Hashem, and M. I. Marei, "Optimized harmonic elimination for cascaded multilevel inverter," in *Power Engineering Conference (UPEC), 2013 48th International Universities*, pp. 1–6, 2013.

[65] T. Tang, J. Han, and X. Tan, "Selective harmonic elimination for a cascade multilevel inverter," in *2006 IEEE International Symposium on Industrial Electronics*, vol. 2, pp. 977-981, 2006.